

Coherent Scattering in Multi-Harmonic Light Microscopy

Laurent Moreaux, Olivier Sandre, Serge Charpak, Mireilles Blanchard-Desce, Jérôme Mertz

▶ **To cite this version:**

Laurent Moreaux, Olivier Sandre, Serge Charpak, Mireilles Blanchard-Desce, Jérôme Mertz. Coherent Scattering in Multi-Harmonic Light Microscopy. Biophysical Journal, 2001, 80 (3), pp.1568-1574. 10.1016/S0006-3495(01)76129-2 . hal-01920233

HAL Id: hal-01920233
https://hal.science/hal-01920233

Submitted on 13 Nov 2018

HAL is a multi-disciplinary open access archive for the deposit and dissemination of scientific research documents, whether they are published or not. The documents may come from teaching and research institutions in France or abroad, or from public or private research centers.

L'archive ouverte pluridisciplinaire **HAL**, est destinée au dépôt et à la diffusion de documents scientifiques de niveau recherche, publiés ou non, émanant des établissements d'enseignement et de recherche français ou étrangers, des laboratoires publics ou privés.

Coherent Scattering in Multi-Harmonic Light Microscopy

Laurent Moreaux,* Olivier Sandre,† Serge Charpak,* Mireille Blanchard-Desce,‡ and Jerome Mertz*
*Laboratoire de Neurophysiologie INSERM EPI 00-02, ESPCI, Paris, †Laboratoire Physico-Chimie CNRS UMR 168, Institut Curie, Paris, and ‡Laboratoire Synthèse et Electrosynthèse Organique CNRS UMR 6510, Université de Rennes, Rennes, France

ABSTRACT By focusing a pulsed laser beam into a sample, harmonic up-conversion can be generated as well as multi-photon excited fluorescence. Whereas multi-photon excited fluorescence microscopy is well established, the use of multi-harmonic generation for three-dimensional image contrast is very recent. Both techniques can provide similar resolution and, for adequate radiating source density, comparable signal levels, allowing them to be combined in a single versatile instrument. However, harmonic generation differs fundamentally from fluorescence generation in that it is coherent and produces radiation patterns that are highly sensitive to phase. As such, multi-harmonic generation microscopy provides a unique window into molecular spatial organization that is inaccessible to fluorescence.

INTRODUCTION

In standard fluorescence microscopy, molecular excitation is caused by the absorption of a single photon. It has been recognized, however, that molecular excitation by the absorption of two or more photons can often be advantageous for specific imaging applications. This has given rise to the techniques of two-photon (Denk et al., 1990) and three-photon (Maiti et al., 1997) microscopy (2PEF and 3PEF, respectively), or, more generally, multi-photon excited fluorescence (MPEF) microscopy (Xu et al., 1996). Alternatively, nonlinear microscopy can be extended to the use of multi-harmonic light wherein the energy of incident photons instead of being absorbed by a molecule, is scattered via a process of harmonic up-conversion (Bloembergen, 1965). As in the case of fluorescence, the use of second (Hellwarth and Christensen, 1974; Gannaway and Sheppard, 1978; Gauderon et al., 1998; Guo et al., 1997; Lewis et al., 1999; Campagnola et al., 1999) or third harmonic generation (Muller et al., 1998; Yelin and Silberberg, 1999) (2HG and 3HG, respectively) opens the field to multi-harmonic generation (MHG) microscopy. Demonstrations of three-dimensional imaging with harmonic up-conversion are very recent and have served largely as proof of principle. We present the fundamental properties of MHG microscopy, with emphasis on its difference from fluorescence microscopy, and demonstrate some powerful applications of second harmonic microscopy in the imaging of biological membranes.

Received for publication 22 June 2000 and in final form 22 November 2000.

Address reprint requests to Jerome Mertz, Laboratoire de Neurophysiologie, INSERM EPI 00-02, ESPCI, 10 rue Vauquelin, 75005 Paris, France. Tel.: 33-1-4079-4761; Fax: 33-1-4079-4760; E-mail: jerome.mertz@espci.fr.

© 2001 by the Biophysical Society

0006-3495/01/03/1568/07 $2.00

THEORY

Multi-harmonic scattering cross-sections

Molecular harmonic up-conversion originates from the nonlinear dependence of the induced molecular dipole moment μ on a driving optical electric field E. We can write

$$\mu = \mu_0 + \alpha \cdot \mathrm{E} + \tfrac{1}{2}\beta{:}\mathrm{EE} + \tfrac{1}{6}\gamma{:}\mathrm{EEE} + \ldots \qquad (1)$$

where α is the linear molecular polarizability and β and γ are the nonlinear first and second hyperpolarizabilities (Bloembergen, 1965; Chemla and Zyss, 1984). The 2HG is governed by β, whereas 3HG and 2PEF are governed by γ. Considerable efforts have been made to engineer molecules with large nonlinear hyperpolarizabilities (Marder et al., 1991; Blanchard-Desce et al., 1997; Kuzyk and Dirk, 1990). A class of molecules known as push-pull chromophores has been shown to be particularly effective for both 2HG and 2PEF (Kogej et al., 1998; He et al., 1995). These molecules consist of donor and acceptor endgroups connected by a charge conjugation path, occasioning the possibility of a large charge transfer along the molecular axis upon excitation. Because we will directly compare the radiated powers produced by MHG and by MPEF, we introduce the following molecular harmonic scattering cross-sections:

$$\sigma_{2\mathrm{HG}} = \frac{4\hbar\omega^5}{3\pi n\varepsilon_0^3 c^5}|\beta|^2 \quad [\mathrm{m}^4(\mathrm{photon/s})^{-1}] \qquad (2)$$

$$\sigma_{3\mathrm{HG}} = \frac{3\hbar^2\omega^6}{2\pi n^2\varepsilon_0^4 c^6}|\gamma|^2 \quad [\mathrm{m}^6(\mathrm{photon/s})^{-2}] \qquad (3)$$

where we assume that the molecule is uni-axial, meaning that its hyperpolarizability tensor is dominated by a single component in the molecule frame of reference. We further assume that the molecule is aligned parallel to the driving field polarization (ω = fundamental driving frequency; n = refractive index). These cross-sections are defined in the same units as the corresponding MPEF cross-sections of the same order (Xu et al., 1996; Xu and Webb, 1996), and directly provide the multi-harmonic scattered power from a single molecule for a given driving field intensity.

MHG from focused beams

Molecules that undergo MPEF may be regarded as independent radiating sources because they produce fluorescence light with random phase. That is, the total emitted fluorescence power scales as the number of radiating molecules. In contrast, the phase of the radiated harmonic light is tightly matched to the phase of the driving fundamental light, meaning that molecules contributing to MHG may no longer be regarded as independent

sources and the total radiated harmonic power becomes critically dependent on both the spatial distribution of the molecules and of the driving field. Most experiments and indeed most theories involving MHG are specifically based on the use of a collimated driving field that possesses a well defined propagation direction and uniform longitudinal intensity (Shen, 1984). On the other hand, if MHG is intended to provide images of microscopic resolution, then the driving field must be tightly focused. The driving field then necessarily contains a wide range of propagation directions in addition to a greatly enhanced intensity near the focal center. The implications of tight focusing on MHG are quite dramatic and require a substantial revision of the theory for collimated beams. First, the active surface (or volume) from which essentially all the multi-harmonic light is generated becomes highly confined about the focal center. Such an inherent confinement is familiar from MPEF, and the active surfaces (or volumes) in both cases may be defined identically (Mertz, 1998). Where MHG and MPEF differ, however, stems from considerations of phase. A well-known particularity of a focused light beam is that its phase is shifted by a half-cycle upon propagation through its focal center. This phenomenon, commonly referred to as a Gouy shift or phase anomaly (Born and Wolf, 1993), produces an effective dilation of the light wavelength near the focal center. As a result, multi-harmonic light generated by a focused driving beam is largely prevented from propagating in the forward direction because of phase matching, and is forced to propagate off-axis.

In order to properly quantify the nature of MHG emission for molecular and driving field distributions that can vary on microscopic scales, a conventional theory based on macroscopic nonlinear susceptibilities is found to be inadequate, and instead we develop a more refined model wherein individual molecules scatter the driving field according to their MHG scattering cross-sections (see above), and their resultant electric field contributions in the radiation zone are summed in the same manner as for phased-array antennas (Krauss, 1950). We consider two geometries of particular relevance: surface geometries, occasioned when imaging biological membranes, and volume geometries. Because 2HG requires asymmetrical radiation sources, it is usually reserved to surface geometries, which can impose high degrees of molecular orientation. Moreover, because spatial symmetry is broken in the direction perpendicular to the surface, 2HG is most effective for a driving field propagation direction parallel to the surface (Moreaux et al., 2000a). On the other hand, 3HG may be produced from either asymmetrical or symmetrical sources, and hence may occur in volumes where molecules are oriented randomly. In both cases, MHG propagation in the forward direction is found to be largely prohibited, and the emission pattern is confined to twin lobes in the case of surface generation, as has been confirmed experimentally (Moreaux et al., 2000b), or a cone in the case of volume generation (see Fig. 1). The lobes or cone are highly peaked at an off-axis angle which is critically dependent on the Gouy shift resulting from the tight focus of the driving field (Moreaux et al., 2000b). In the case of a focused driving field with an aperture-limited angular distribution of half-width θ_0, the outgoing multi-harmonic radiation is peaked at the approximate off-axis angles $\pm\theta_0/\sqrt{2}$ for a surface geometry and $\theta_0/2$ for a volume geometry. We observe that essentially all the harmonic light may be detected provided one uses collection optics in the forward direction with a wide enough angular aperture. In contrast, fluorescence light which is radiated equally in the forward and backward directions is usually collected in an epifluorescence geometry with considerably smaller collection efficiencies, typically much less than 50%. The combination of both forward and backward detection naturally allows the capacity for simultaneous harmonic and fluorescence imaging.

The total radiated MHG power is derived by integrating the radiation profile over all the emission directions. We find, for m = 2, 3, . . .

$$P_{\mathrm{mHG}} = \frac{1}{\mathrm{m}}\,\Theta_{\mathrm{m}} N^2 \sigma_{\mathrm{mHG}} I_0^{\mathrm{m}} \tag{4}$$

where I_0 is the driving field intensity at the focal center, N is the effective number of radiating molecules, and Θ_{m} is a parameter which will be defined below. We determine N by first quantifying the surface area S or the volume V which encompasses essentially all the MHG, and assuming that the labeling density is approximately spatially uniform. In cases of moderate to tight focusing (numerical aperture >0.8) the active surface or volume may be approximated by $S \approx 9\, w_0^3/\lambda$ for 2HG or $V \approx 6\, w_0^4/\lambda$ for 3HG, where w_0 is the beam waist at the focus and λ the wavelength of the fundamental beam in the sample medium, obtaining $N = SN_{\mathrm{S}}$ or $N = VN_{\mathrm{V}}$ (N_{S} and N_{V} are the molecular surface and volume densities, respectively). We note that the radiated fields from these N molecules are not necessarily in phase with one another because the molecules are distributed over an area whose dimensions are at least of order λ. As a result, the total power

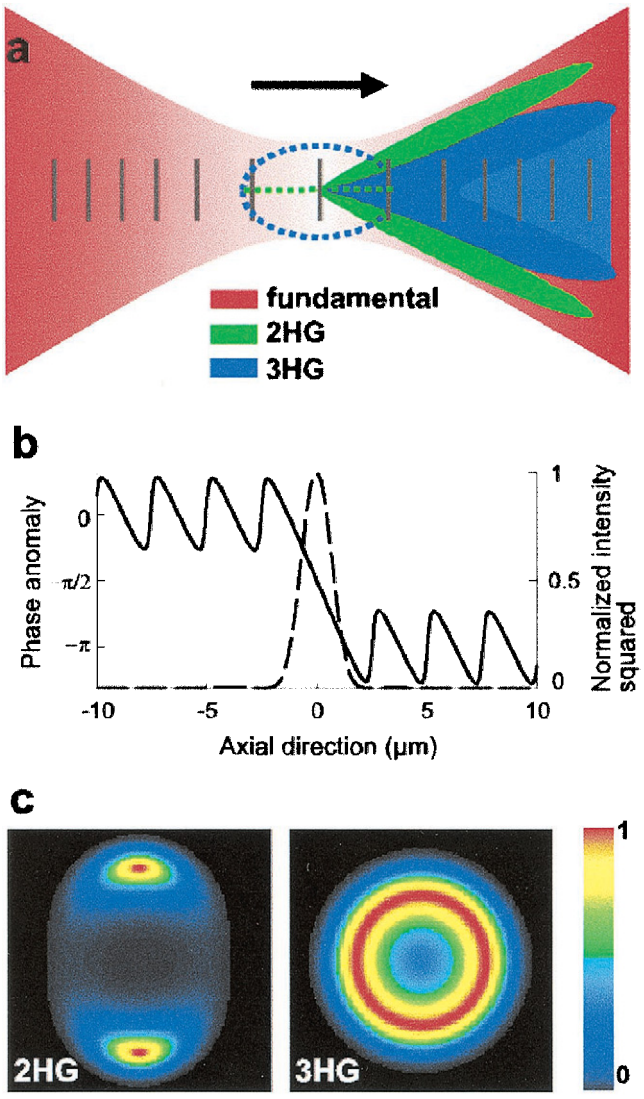


FIGURE 1 A fundamental driving field (red) is tightly focused to a microscopic spot size (*a*). Phase-matching forces the multi-harmonic radiation pattern to be twin-lobed in the case of surface generation (green), and conical in the case of volume generation (blue). Middle traces (*b*) display the on-axis phase (*solid*) and intensity (*dashed*) variations of the driving field near its focal center. These govern, respectively, the phase-matching and its interaction area or volume of MHG. The traces are derived from full numerical calculations for 880 nm light focused with a water-immersion 0.9 numerical aperture objective. MHG emission patterns are also shown head-on (*c*).

radiated by these molecules is substantially reduced compared to the power they would radiate if they were all perfectly in phase. The parameter Θ_m corresponds precisely to this reduction factor. For conditions where the focal tightness is moderate, we may approximate $\Theta_2 \approx (0.1\ \lambda/w_0)^2$ and $\Theta_3 \approx (0.01\ \lambda/w_0)^2$, which, as predicted, are both significantly smaller than 1. Based on these approximations, we find that $\Theta_2 N^2 \approx 0.8\ w_0^4 N_S^2$ and $\Theta_3 N^2 \approx 3 \times 10^{-3}\ w_0^6 N_V^2$. Recalling finally that I_0 scales as w_0^{-2}, we observe that the total powers radiated by surface 2HG and by volume 3HG are roughly independent of focal tightness. This result is similar to that obtained for 2PEF in volume only.

MHG versus MPEF

We can directly compare the respective powers obtained by multi-harmonic and fluorescence generation by using the estimate $P_{mHG}/P_{mPEF} \approx 2^{d/2}\ \Theta_m N(\sigma_{mHG}/\sigma_{mPEF})$, which supposes the two generation processes are independent ($d = 2, 3$ is the number of spatial dimensions). In practice, σ_{mHG} is usually much smaller than σ_{mPEF} for a single molecule, a fact which may appear as an impasse for MHG microscopy. By exciting a molecule near resonance, however, we may enhance σ_{mHG}, typically up to 1 to 2 orders in magnitude. Moreover, we observe that MHG scales quadratically with N, whereas fluorescence scales only linearly with N. As an example, 2HG and 2PEF cross-sections of Di-6-ASPBS (N-(4-sulfobutyl)-4-(4-(dihexylamino) styryl)pyridinium, synthesized in our lab) inserted in a membrane are compared in Fig. 2. To obtain σ_{2HG}, the hyperpolarizability of the molecule along the charge-transfer axis is estimated roughly from a two-state model (Chemla and Zyss, 1984; Shen, 1984; Loew and Simpson, 1981; Moreaux et al., 2000b) (charge-transfer energy ≈2.6 eV, transition moment ≈10 D, change in dipole moment between the ground state and excited-state ≈16 D, damping factor ≈0.2 eV). The 2PEF cross-section of Di-6-ASPBS is inferred from 2PEF measurements in ethanol, which are corrected to take into account the reported blue-shift in the one-photon absorption spectrum and quantum yield increase when the molecule is inserted in the membrane (Fluhler et al., 1985). For a driving wavelength of 880 nm, the cross-sections are estimated to be $\sigma_{2HG} \approx 1 \times 10^{-3}$ GM and $\sigma_{2PEF} \approx 30$ GM (Fig. 2), obtaining $\sigma_{2HG}/\sigma_{2PEF} \approx 10^{-4}$. The labeling density needed to yield approximately equivalent 2HG and 2PEF powers, given by $N_S \approx 5/\lambda w_0\ (\sigma_{2PEF}/\sigma_{2GH})$, then corresponds to ~1 mol% ($N \approx 2 \times 10^4$). Such density is routinely used for the membrane staining of live cells. We emphasize that an equivalency in signal levels is highly desirable for combined 2HG and 2PEF microscopy because it allows compatible integration times and, hence, compatible scanning speeds. In other words, the detection of 2HG in no way hampers the detection of 2PEF, and the two modes can independently provide comparable image qualities. (For approximately equivalent 3HG and 3PEF powers, the required labeling density is $N_V \approx 700/\lambda w_0^2\ (\sigma_{3PEF}/\sigma_{3HG})$.)

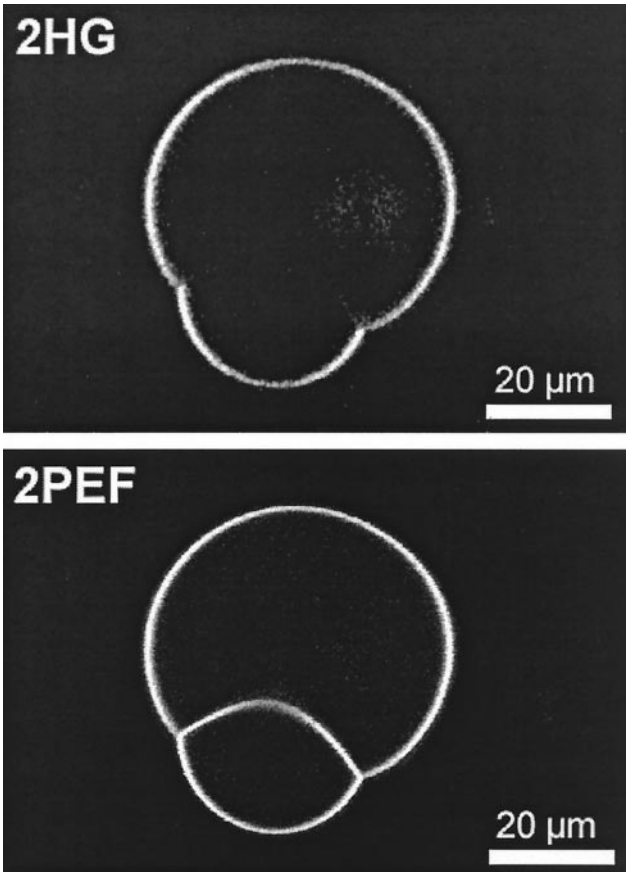


FIGURE 3 Simultaneous 2HG and 2PEF images of adhering GUVs whose outer membrane leaflets are labeled with Di-6-ASPBS. Because dye molecules are symmetrically distributed in the adhesion zone, 2HG is forbidden, whereas 2PEF is not. The laser excitation was linearly polarized along the horizontal axis and delivered <1 mW at the sample. The pixel integration time was 40 μs.

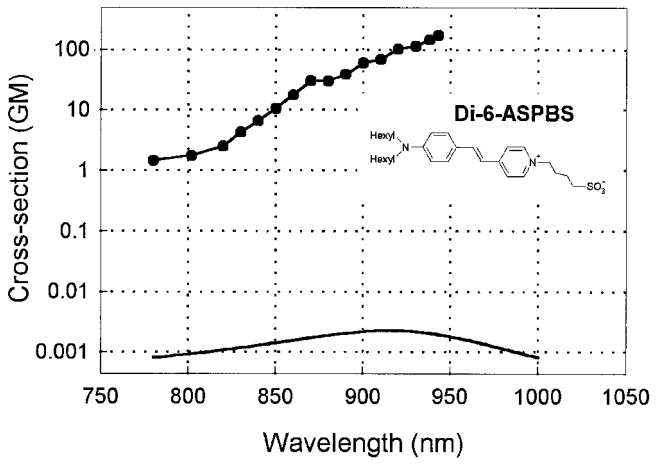


FIGURE 2 Semi-experimental estimations of 2HG (*solid trace*) and 2PEF (*closed circles*) cross-sections of Di-6-ASPBS inserted in a membrane (1 GM = 10^{-50} cm^4/photon s^{-1}). The 2HG cross-sections are derived from measured parameters applied to a two-state model. The 2PEF cross-sections are inferred from measurements in ethanol, corrected for an absorption blue-shift and quantum yield increase in a membrane environment.

RESULTS AND DISCUSSION

In order to demonstrate some capacities unique to 2HG microscopy that are inaccessible to fluorescence, we built a combined MHG-MPEF upright scanning microscope. The excitation source was a mode-locked Ti:sapphire laser (Spectra-Physics) delivering ~80-fs pulses at 81 MHz, and operated at 880 nm wavelength. The microscope consisted of galvanometer mounted mirrors (GSI Lumonics) for en-face scanning, and a water immersion objective (Olympus 60× NA = 0.9) mounted on a motorized translation stage (Physik Instrumente). The emitted harmonic and fluores-

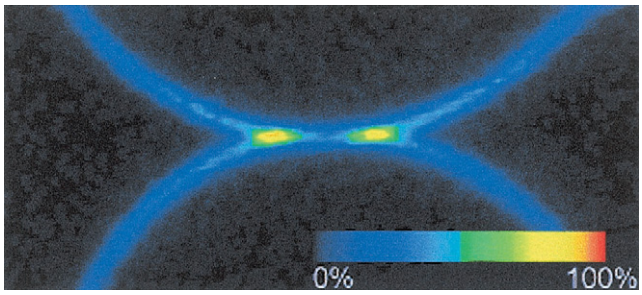


FIGURE 4 Two GUVs are brought into close proximity, occasioning partial destructive or constructive interference of the 2HG signal depending on the separation of the GUV membranes. 2HG provides an accurate measure of the local separation for distances smaller than the focal spot size of the excitation beam. The illumination power is <1 mW.

cence light were isolated with interference filters (Chroma) and detected with photomultiplier tubes (Hamamatsu). The microscope control and signal acquisition were performed via a computer interface board (National Instruments).

Coherence properties of 2HG radiation

Because 2HG requires a non-centrosymmetrical radiating source, it serves as a sensitive measure of local molecular orientation. We used giant unilamelar vesicles (GUVs) as model lipid bilayers, whose outer leaflets were labeled with an extravesicular perfusion of 2 μM Di-6-ASPBS. (Preparation and labeling are described in Sandre et al., 1999). Fig. 3 illustrates simultaneous 2PEF and 2HG cross-sectional images of two GUVs that have undergone adhesion. In the adhesion zone, the molecular distribution is centro-symmetrical because an approximately equal number of molecules are oriented in opposing directions and hence produce 2HG with opposing phases. This leads to a total destructive interference of 2HG, whereas it produces no change in phase-insensitive fluorescence.

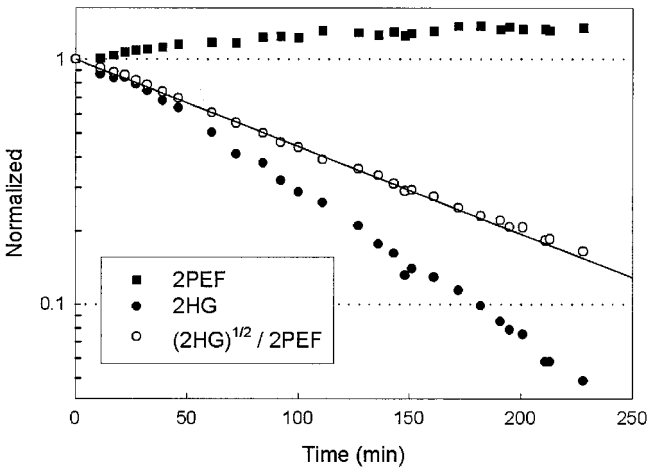


FIGURE 5 The dynamics of Di-6-ASPBS flip-flop in a bilipid membrane initially labeled in the outer leaflet only. 2HG (*closed circles*) provides a signature of local molecular orientation which may be corrected for local concentration variations monitored by 2PEF (*closed squares*). The open circles represent the fraction of molecules that are asymmetrically distributed. The time constant for Di-6-ASPBS flip-flop at room temperature is observed to be about 2 h.

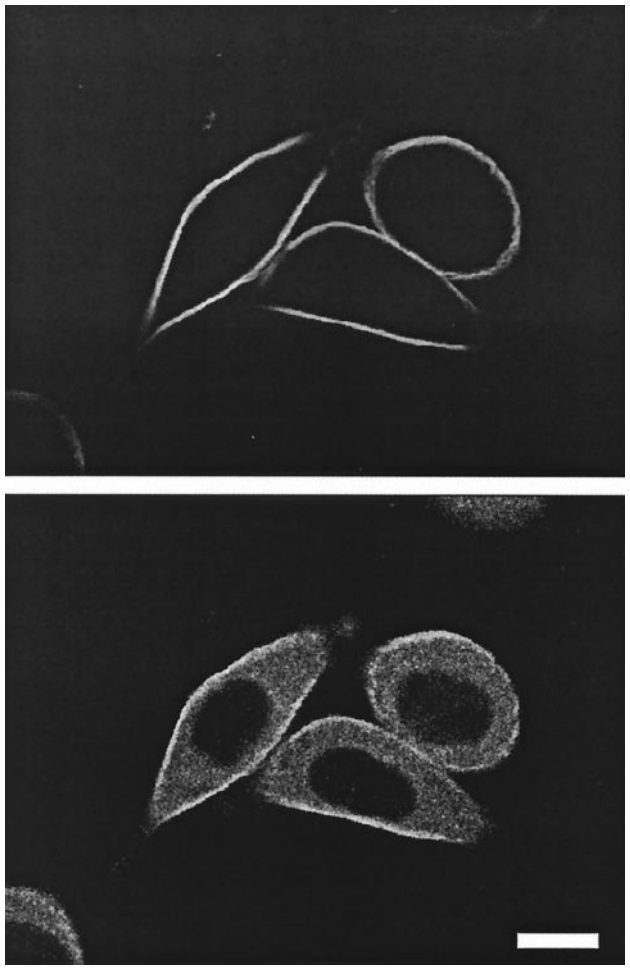


FIGURE 6 Simultaneous 2HG (*top*) and 2PEF (*bottom*) cross-sectional images of isolated Ncad1 cells labeled with RH237. Internalized dye molecules become randomly oriented in the cytoplasm and generate no 2HG, whereas they continue to generate fluorescence. The laser excitation was linearly polarized and the power at the sample was ~1 mW. Three images were averaged, each with 10 μs pixel integration time and 120° rotated polarization directions. Scale bars are 15 μm.

The theory of phased emission in MHG may be readily applied to more complicated geometries than a single membrane plane. In particular, when two membranes approach one another to within a proximity smaller than the microscopic resolution, then 2HG can serve as an accurate measure of their local separation for distance ranges under w_0. In Fig. 4, two labeled GUVs are brought into close proximity without adhesion, occasioning partial destructive interference of 2HG at the near contact point. With increasing membrane separation, the 2HG signal increases approximately linearly and becomes maximum at a separation of

$\sim 0.6\ w_0$, at which point the 2HG interference is constructive (in our case, $w_0 = 510$ nm). Beyond this separation, the two membranes can no longer be simultaneously illuminated within the same focal spot, and hence their 2HG signals become independent. The range of separation distances that can be measured by 2HG is of particular interest, since it is inaccessible to ordinary diffraction limited imaging, and is also inaccessible to measurements involving fluorescence resonant energy transfer (FRET), which are very short-ranged (Weiss, 1999). As a result, 2HG effectively bridges the gap between these techniques. We emphasize here that the observation of hot spots of constructive interference corroborates the fact that the 2HG is directed off-axis. If the 2HG were directed strictly on-axis, these hot spots would not occur.

Finally, the requirement of a non-centrosymmetrical radiating source for 2HG provides a unique window into the study of membrane dynamics. As shown above, a lipid bilayer labeled with Di-6-ASPBS only in its outer (or inner) leaflet produces both 2HG and fluorescence. Over long times, however, this labeling becomes thermally redistributed by molecular flip-flop into both leaflets (Srivastava and Eisenthal, 1998), and the net molecular distribution becomes progressively more centrosymmetrical, causing a decay in the 2HG signal, as demonstrated in Fig. 5. The simultaneously acquired 2PEF signal is insensitive to flip-flop and reflects only variations in the dye concentration, presumably owing to slow labeling dynamics. Hence, an accurate measure of local molecular orientation dynamics is obtained by monitoring the 2HG signal and correcting for local concentration variations, which are monitored by 2PEF.

Biological membrane imaging

We illustrate the remarkable specificity of 2HG for the imaging of cell membranes. The images in Fig. 6 represent simultaneous 2HG and 2PEF images of mouse sarcoma S180 cells genetically modified to express N-cadherin (Dufour et al., 1999). The cells were labeled by an extracellular perfusion of 1 μM RH237 (Grinvald et al., 1982) (N-(4-sulfobutyl)-4-(6-(4-(dibutylamino)phenyl)hexatrienyl)pyridinium, synthesized in our lab). We note here that RH237 has a longer polyenic chain than Di-6-ASPBS and was observed to be more efficient at 2HG, though less efficient at 2PEF. As is apparent from the fluorescence images, some of the dye has been internalized into the cell cytoplasm. Upon internalization, the dye molecules become randomly oriented and, hence, produce no coherent 2HG, resulting in highly contrasted images where only the cell membranes are visible. Cell viability was confirmed by subsequent observation of cellular division.

Figure 7 illustrates labeled neurons in an organotypic brain slice (Gähwiler, 1988). The labeling was performed by depositing a small RH237 crystal below the glial cell surface layer and incubating overnight at 36°C. Whereas dye internalization degrades, and in some cases erases the contrast of the membranes in the fluorescence images, it manifestly has no effect on the high contrast in the 2HG images. We note, however, that although no 2HG is produced in intracellular regions, a fair amount of 2HG is still observed in the neuropil, which consists mainly of lipid membranes and apparently imparts some degree of spatial organization at microscopic length scales. To our knowledge, Fig. 7 represents the first 2HG images of neurons in

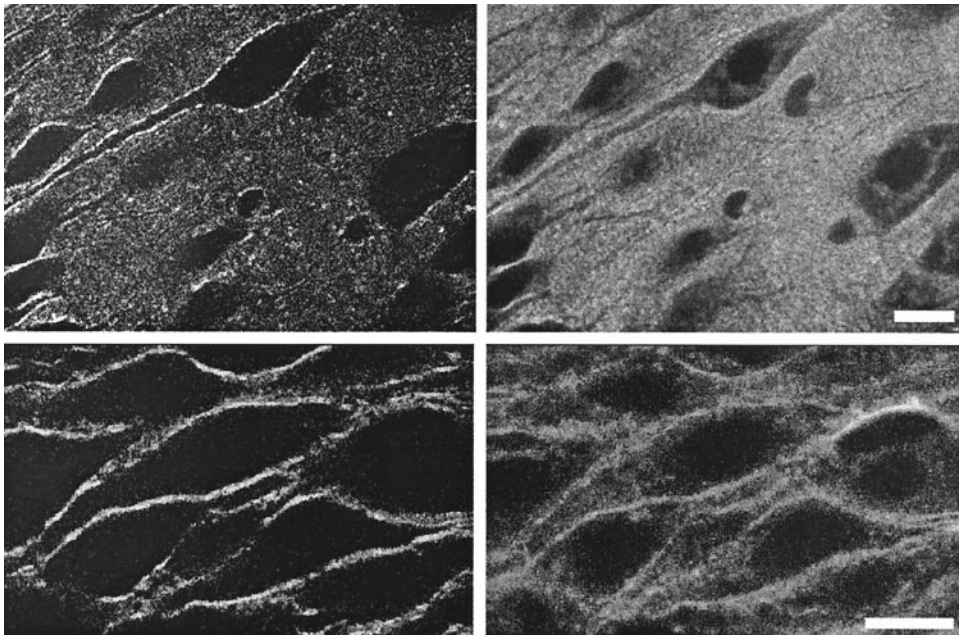


FIGURE 7 (*Top panels*) Simultaneous 2HG (*left*) and 2PEF (*right*) images of a hippocampal slice culture labeled with RH237. Three images were averaged, each with 10 μs pixel integration time and no polarization rotation. Note the enhanced 2HG contrast of the CA1 pyramidal cell walls. (*Bottom panels*) Non-averaged images of the pyramidal layer in the same slice. The slice was <100 μm thick. The laser power at the sample was <5 mW. Scale bars are 15 μm.

physiological environments that preserve anatomical structure.

CONCLUSION

We emphasize that the molecules used in this work are already well known with regard to their properties of electrochromism (Grinvald et al., 1982; Fluhler et al., 1985) and have been extensively used as fluorescent reporters of membrane potential, e.g., in organotypic (Bolz et al., 1992) slices similar to those illustrated in Fig. 7. Only recently, however, has their ability to produce efficient 2HG been applied to microscopic imaging, and their capacities remain largely untapped. For example, MHG may serve as an effective contrast signature for static electric fields or microenvironment polarity. In particular, styryl dyes producing 2HG have been reported to be up to an order of magnitude more responsive than the best fluorescent indicators of membrane potential (Bouevitch et al., 1993; Peleg et al., 1999; Campagnola et al., 1999), with the added benefit that their response times are instantaneous. In a different context, 3HG has also been reported to be a viable technique for the imaging of endogenous species without causing photobleaching or saturation, as normally occasioned by fluorescence (Muller et al., 1998; Yelin and Silberberg, 1999) and requires no interface-induced symmetry breaking. Moreover, a high volume density of endogenous species can compensate for the smallness of 3HG cross-sections. Finally, though we have provided here a detailed description of extramolecular processes governing multi-harmonic radiation, a complete account requires a better understanding of the intramolecular mechanisms behind MHG. Recent work on dipolar and quadrupolar dyes promises significant advances in the engineering of markers specifically adapted to nonlinear imaging (Albota et al., 1998; Ventelon et al., 1999), as well as insight into the links between harmonic and fluorescence generation.

We are grateful to S. Dufour for providing us with the Ncad1 cells and to B. Gähwiler for the slice cultures. We also thank W. W. Webb for a careful reading and insightful comments. Finally, we are grateful to the Institut Curie and the CNRS for financial support.

REFERENCES

Albota, M., D. Beljonne, J. L. Brédas, J. E. Ehrlich, J.-Y. Fu, A. A. Heikal, S. E. Hess, T. Kogej, M. D. Levin, S. R. Marder, D. McCord-Maughon, J. W. Perry, H. Röckel, M. Rumi, G. Subramaniam, W. W. Webb, X.-L. Wu, and C. Xu. 1998. Design of organic molecules with large two-photon absorption cross sections. *Science.* 281:1653–1656.

Blanchard-Desce, M., V. Alain, P. V. Bedworth, S. R. Marder, A. Fort, C. Runser, M. Barzoukas, S. Lebus, and R. Wortmann. 1997. Large quadratic hyperpolarizabilities with donor-acceptor polyenes exhibiting optimum bond length alteration. Correlation between structure and hyperpolarizability. *Chem. Eur. J.* 3:1091.

Bloembergen, N. 1965. Nonlinear Optics. World Scientific.

Bolz, J., N. Novak, and V. Staiger. 1992. Formation of specific afferent connections in organotypic slice cultures from rat visual cortex cocultured with lateral geniculate nucleus. *J. Neurosci.* 12:3054–3079.

Born, M., and E. Wolf. 1993. Principles of Optics. Pergamon Press, Oxford.

Bouevitch, O., A. Lewis, I. Pinevsky, J. P. Wuskell, and L. M. Loew. 1993. Probing membrane potential with nonlinear optics. *Biophys. J.* 65: 672–679.

Campagnola, P. J., M. Wei, A. Lewis, and L. M. Loew. 1999. High-resolution nonlinear optical imaging of live cells by second harmonic generation. *Biophys. J.* 77:3341–3349.

Chemla, D. S., and J. Zyss. 1984. Nonlinear Optical Properties of Organic Molecules and Crystals. Academic Press, New York.

Denk, W., J. H. Strickler, and W. W. Webb. 1990. Two-photon laser scanning fluorescence microscopy. *Science.* 248:73.

Dufour, S., A. Beauvais-Jouneau, A. Delouvée, and J. P. Thiery. 1999. Differential function of N-cadherin and cadherin-7 in the control of embryonic cell motility. *J. Cell Biol.* 146:501–516.

Fluhler, E., V. G. Burnham, and M. L. Loew. 1985. Spectra, membrane binding, and potentiometric responses of new charges shift probes. *Biochemistry.* 24:5749.

Gähwiler, B. H. 1988. Organotypic cultures of neural tissue. *Trends Neurosci.* 11:484–489.

Gannaway, J. N., and C. J. R. Sheppard. 1978. Second-harmonic imaging in the scanning optical microscope. *Opt. Quant. Elect.* 10:435–439.

Gauderon, R., P. B. Lukins, and C. J. R. Sheppard. 1998. Three-dimensional second-harmonic generation imaging with femtosecond laser pulses. *Opt. Lett.* 23:1209.

Grinvald, A., R. Hildesheim, I. C. Farber, and L. Anglister. 1982. Improved fluorescent probes for the measurement of rapid changes in membrane potential. *Biophys. J.* 39:301–308.

Guo, Y., P. P. Ho, H. Savage, D. Harris, P. Sacks, S. Schantz, F. Liu, N. Zhadin, and R. R. Alfano. 1997. Second-harmonic tomography of tissues. *Opt. Lett.* 22:1323.

He, G. S., J. D. Jayant, D. Bhawalkar, C. F. Zhao, and P. N. Prasad. 1995. Optical limiting effect in a two-photon absorption dye doped solid matrix. *Appl. Phys. Lett.* 67:2433.

Hellwarth, R., and P. Christensen. 1974. Nonlinear optical microscopic examination of structure in polycrystalline ZnSe. *Opt. Comm.* 12: 318–322.

Kogej, T., D. Beljonne, F. Meyers, J. W. Perry, S. R. Marder, and J. L. Brédas. 1998. Mechanisms for enhancement of two-photon absorption in donor-acceptor conjugated chromophores. *Chem. Phys. Lett.* 298:1–6.

Krauss, J. D. 1950. Antennas. McGraw-Hill, New York.

Kuzyk, M. G., and C. W. Dirk. 1990. Effects of centrosymmetry on the nonresonant electronic third-order nonlinear optical susceptibility. *Phys. Rev. A.* 41:5098.

Lewis, A., A. Khatchatouriants, M. Treinin, Z. Chen, G. Peleg, N. Friedman, O. Bouevitch, Z. Rothman, L. Loew, and M. Sheres. 1999. Second-harmonic generation of biological interfaces: probing the membrane protein bacteriorhodopsin and imaging membrane potential around GFP molecules at specific sites in neuronal cells of *C. elegans*. *Chem. Phys.* 245:133–144.

Loew, L. M., and L. L. Simpson. 1981. Charge shift probes of membrane potential: a probable electrochromic mechanism for ASP probes on a hemispherical lipid bilayer. *Biophys. J.* 34:353.

Maiti, S., R. M. Williams, J. B. Shear, W. R. Zipfel, and W. W. Webb. 1997. Measuring serotonin distribution in live cells with three-photon excitation. *Science.* 24:530–532.

Marder, S. R., D. N. Beratan, and L.-T. Cheng. 1991. Approaches for optimizing the first hyperpolarisability of conjugated organic molecules. *Science.* 252:103.

Mertz, J. 1998. Molecular photodynamics involved in multi-photon excitation fluorescence microscopy. *Eur. Phys. J. D.* 3:53–66.

Moreaux, L., O. Sandre, M. Blanchard-Desce, and J. Mertz. 2000a. Membrane imaging by simultaneous second-harmonic generation and two photon microscopy. (Errata 25:678.) *Opt. Lett.* 25:320–322.

Moreaux, L., O. Sandre, and J. Mertz. 2000b. Membrane imaging by second-harmonic generation microscopy. *J. Opt. Soc. Am. B.* 17: 1685–1694.

Muller, M., J. Squier, K. R. Wilson, and G. J. Brakenhoff. 1998. 3D-microscopy of transparent objects using third-harmonic generation. *J. Microsc.* 191:266.

Peleg, G., A. Lewis, M. Linial, and L. M. Loew. 1999. Non-linear optical measurement of membrane potential around single molecules at selected cellular sites. *Proc. Natl. Acad. Sci. USA.* 96:6700–6704.

Sandre, O., L. Moreaux, and F. Brochard. 1999. Dynamics of transient pores in stretched vesicles. *Proc. Natl. Acad. Sci. USA.* 96: 10588–10596.

Shen, Y. R. 1984. The Principles of Nonlinear Optics. Wiley, New York.

Srivastava, A., and K. B. Eisenthal. 1998. Kinetics of molecular transport across a liposome bilayer. *Chem. Phys. Lett.* 292:345–351.

Ventelon, L., L. Moreaux, J. Mertz, and M. Blanchard-Desce. 1999. New quadrupolar fluorophores with high two-photon excited fluorescence. *Chem. Commun.* 20:2055–2057.

Weiss, S. 1999. Fluorescence spectroscopy of single biomolecules. *Science.* 283:1676–1683.

Xu, C., and W. W. Webb. 1996. Measurement of 2-photon excitation cross-section of molecular fluorophores with data from 690 nm to 1050 nm. *J. Opt. Soc. Am. B.* 13:481–491.

Xu, C., W. Zipfel, J. B. Shear, R. M. Williams, and W. W. Webb. 1996. Multiphoton fluorescence excitation: new spectral windows for biological nonlinear microscopy. *Proc. Natl. Acad. Sci. USA.* 93:10763–10768.

Yelin, D., and Y. Silberberg. 1999. Laser scanning third-harmonic-generation microscopy in biology. *Opt. Express.* 5:169.